PHYSICAL REVIEW C VOLUME 23, NUMBER 5 MAY 1981

# Fusion excitation functions for $^{16}O + ^{27}Al$ and $^{16}O + ^{24}Mg$ collisions

K. R. S. Devi
*Kellogg Radiation Laboratory, Caltech, Pasadena, California 91125*

A. K. Dhar
*Daresbury Laboratory, Science Research Council, Warrington, WA4 4AD, United Kingdom*

M. R. Strayer
*A. W. Wright Nuclear Structure Laboratory, Yale University, New Haven, Connecticut 06520*

(Received 24 September 1980)

Fusion excitation functions have been calculated for the $^{16}O + ^{27}Al$ and $^{16}O + ^{24}Mg$ collisions using the time-dependent Hartree-Fock theory. The theoretical results are in good agreement with experiment and predict the existence of a lower angular momentum limit to fusion for $E_{lab} \geq 100$ MeV.

[NUCLEAR REACTIONS $^{16}O + ^{24}Mg$ and $^{16}O + ^{27}Al$ fusion excitation functions in the time-dependent Hartree-Fock approximation.]

## I. INTRODUCTION

Since the initial one dimensional time-dependent Hartree-Fock (TDHF) calculations for colliding slabs,[1] a variety of successively more realistic calculations have been performed for the study of heavy-ion collisions. These studies have primarily focused on the fusion characteristics in heavy-ion reactions with composite mass less than 100,[2-10] deep inelastic aspects in the reactions with composite mass greater than 200,[11-15] and a combination of both in the intermediate mass region.[16,18] The agreement with experiment of some of these calculations illustrates the usefulness of a parameter-free microscopic description of heavy-ion phenomena.

However, in spite of the merits of TDHF calculations, there remain ambiguities arising from the various symmetries and approximations necessary for the solution of the TDHF equations. Thus full three-dimensional TDHF calculations for the systems $^{12}C + ^{12}C$,[9] $^{16}O + ^{16}O$,[2-4] $^{16}O + ^{40}Ca$,[10] and $^{40}Ca + ^{40}Ca$ (Ref. 4) have been performed, assuming spin-isospin degeneracy of the single-particle states and a simplified local Skyrme-type force with no spin-orbit interaction. Although in most of the subsequent calculations a nonlocal Skyrme interaction,[19] with the isospin degeneracy relaxed, has been used, the TDHF equations have been reduced to two nontrivial dimensions[20,21] by enforcing a symmetry about the line joining the centers of mass of the reacting ions. This approximation is exact for head-on collisions and is possibly only approximately valid at low bombarding energies and also for very heavy systems.[11-14] This imposed axial symmetry constraint restricts equilibration into other degrees of freedom and inhibits locally the angular momentum transfer between the reacting partners. Consequently, the fragments tend to be left deformed and the reactions less relaxed. In contrast, it has been shown that a frozen approximation,[22,23] in which the components of the single particle wave functions normal to the scattering plane are assumed to be constant in time, closely reproduces the results of three-dimensional calculations[23] at all impact parameters. However, at very high energies, there are reported anomalies which indicate that this approximation may be breaking down.[10] These were reported in $^{28}Si + ^{28}Si$ at c.m. energies of 100 MeV and greater. Here, "islands" of nonfusion events were found in the fusion region. These islands were subsequently shown to be spurious and fusion cross sections were obtained by assuming a continuous region of fusion events between a lower and upper angular momentum cutoff. In this paper we have employed the two-dimensional frozen approximation for the study of fusion excitation functions in the $^{16}O + ^{27}Al$ and $^{16}O + ^{24}Mg$ reactions at laboratory energies up to 200 MeV. At the higher energies we have examined the entire region of entrance channel angular momenta with no observed breakdown as reported in Ref. 10. Details of these results are given in Sec. IV.

The effective interaction used in these calculations is the nonlocal, finite range Skyrme II force[19] with no spin-orbit interaction. Fully three-dimensional fusion excitation functions for $^{16}O + ^{16}O$ and $^{40}Ca + ^{40}Ca$ have been calculated using the Bonche-

 

Koonin-Negele (BKN) force and are quantitatively in good agreement with the experimental data.[4] Studies comparing fusion with the BKN force and the Skyrme II force in both $^{16}O$ and $^{40}Ca$ systems demonstrate an enhancement for the latter of about 10% in the fusion cross section at c.m. energies up to about 0.4 MeV per particle above the Coulomb barrier.[6] At energies of about 1 MeV per particle above the Coulomb barrier in $^{16}O+^{40}Ca$ reactions, these forces give the same fusion cross section to better than 20%.[10] However, this comparison is not unambiguous since it involves different methods and approximations. The use of the Skyrme II force gives a good description of many static properties for a wide range of nuclei. TDHF calculations of this type have recently been performed for the reactions $^{16}O+^{93}Nb$,[16] $^{40}Ar+^{58}Ni$,[24] and $^{86}Kr+^{139}La$ in contrast with other studies[20] where very simplified Skyrme-type interactions have been used. Even though our calculation represents the first detailed study of fusion in light asymmetric systems with a full Skyrme interaction, we find no qualitatively different results from those established with the original BKN force.

## II. CALCULATIONAL DETAILS

The details of the frozen approximation have been described in Refs. 22 and 25. Here we only briefly summarize the relevant results. Assuming that the collision involves two fragments, the TDHF single particle wave functions $\psi_\lambda$ at any instant of time $t$ can be written as[22]

$$\psi^q_\lambda(\vec{r},t)=\chi_\eta(\vec{r}_\perp)\,\phi^q_{\lambda\eta}(\vec{r}_\parallel,t), \tag{1}$$

where $\vec{r}_\parallel$ are the coordinates in the reaction plane and $\vec{r}_\perp$ are those in a direction perpendicular to the reaction plane. The superscript $q$ denotes the charge state of the particle. The component of the wave function perpendicular to the reaction plane $\chi_\eta(\vec{r}_\perp)$ is assumed to be time independent and is taken to be a one dimensional harmonic oscillator function with quantum number $\eta$. The TDHF equations are then obtained by minimizing the many particle action

$$\mathcal{S}=\int dt[\langle\Psi|H|\Psi\rangle-i\hbar\langle\Psi|\dot{\Psi}\rangle] \tag{2}$$

under the assumption that the many body wave function is a Slater determinant of single particle wave functions $\psi^q_\lambda(\vec{r},t)$ given by Eq. (1). The action $\mathcal{S}$ is first integrated over $\vec{r}_\perp$ and the resulting expression (which involves only $\phi^q_{\lambda\eta}$) is minimized with respect to $\phi^q_{\lambda\eta}$ to give

$$h^q_\eta(\vec{r}_\parallel,t)\phi^q_{\lambda\eta}(\vec{r}_\parallel,t)=i\hbar\dot{\phi}^q_{\lambda\eta}(\vec{r}_\parallel,t), \tag{3}$$

where $h^q_\eta(\vec{r}_\parallel,t)$ is the one body TDHF Hamiltonian. The modifications of Eq. (3) for discrete space and time mesh and the techniques for solving these are discussed in Refs. 16 and 25.

## III. INITIAL CONDITIONS

The initial wave functions for the solution of TDHF equations [Eq. (3)] are taken to be those corresponding to the HF ground states of the reacting partners, boosted towards each other with an appropriate initial relative velocity. The ions are assumed to move from infinity to some relatively large separation (about 12 fm) chosen at time $t=0$ along classical Coulomb trajectories.

The static Hartree-Fock solutions were generated using the imaginary time method.[17] For the $^{16}O$ nucleus the neutrons and protons completely fill the $0s$ and $0p$ shells and hence the HF state is spherically symmetric. For $^{24}Mg$ and $^{27}Al$ the filling approximation is employed according to which the density matrix is written as

$$\rho(\vec{r},\vec{r}',t)=\sum_\lambda W_\lambda\,\psi_\lambda(\vec{r},t)\psi^*_\lambda(\vec{r}',t),$$

where $W_\lambda$'s are the time independent occupation numbers. This prescription gives spherical HF ground states for these nuclei.

However, one of the questions that remains unanswered in this study (as well as other calculations) pertains to the role played by the filling approximation. This approximation leads to a partial filling of some of the single particle states and hence to the deviation from a single Slater determinantal nature of the TDHF wave functions. As a consequence, the initial conditions for the TDHF calculations are different from those obtained with deformed static Hartree-Fock wave functions. Giving up the filling approximation leads to deformed Hartree-Fock shapes for $^{27}Al$ and $^{24}Mg$. So far, the effect of entrance channel

TABLE I. Single particle orbits for the valence nucleons of $^{27}Al$ and $^{24}Mg$. $W_\lambda$'s are occupation numbers and $\eta$, $\{\mu,\nu\}$ are the initial oscillator quantum numbers in the $\vec{r}$ and $\{\vec{r}\}$ directions, respectively.

| $W_\lambda^{\text{neutron}}$ | $W_\lambda^{\text{proton}}$ | $\eta$ | $\mu$ | $\nu$ | $W_\lambda^{\text{neutron}}$ | $W^{\text{proton}}$ | $\eta$ | $\mu$ | $\nu$ |
|---|---|---|---|---|---|---|---|---|---|
| 1 | $\frac{5}{6}$ | 0 | 1 | 1 | $\frac{2}{3}$ | $\frac{2}{3}$ | 0 | 1 | 1 |
| 1 | $\frac{5}{6}$ | 1 | 0 | 1 | $\frac{2}{3}$ | $\frac{2}{3}$ | 1 | 0 | 1 |
| 1 | $\frac{5}{6}$ | 1 | 1 | 0 | $\frac{2}{3}$ | $\frac{2}{3}$ | 1 | 1 | 0 |
| 1 | $\frac{5}{6}$ | 0 | 2 | 0 | $\frac{2}{3}$ | $\frac{2}{3}$ | 0 | 2 | 0 |
| 1 | $\frac{5}{6}$ | 0 | 0 | 2 | $\frac{2}{3}$ | $\frac{2}{3}$ | 0 | 0 | 2 |
| 1 | $\frac{5}{6}$ | 2 | 0 | 0 | $\frac{2}{3}$ | $\frac{2}{3}$ | 2 | 0 | 0 |

TABLE II. Static properties of $^{27}$Al, $^{24}$Mg, and $^{16}$O. Column *a* corresponds to the spherical HF solutions and column *b* to the true deformed HF solutions for $^{27}$Al and $^{24}$Mg.

| Static properties | $^{27}$Al | | | $^{24}$Mg | | | $^{16}$O | |
|---|---|---|---|---|---|---|---|---|
| | *a* | *b* | expt. | *a* | *b* | expt. | *a* | expt. |
| Binding energy (MeV) | −165.573 | −187.714 | −225.0 | −141.934 | −165.439 | −189.387 | −122.484 | −127.6 |
| Kinetic energy (MeV) | 463.878 | 463.905 | | 404.531 | 400.702 | | 243.199 | |
| Nuclear potential energy (MeV) | | | | | | | | |
| (1) Zero range | 302.521 | 299.338 | | 251.436 | 245.165 | | 139.584 | |
| (2) Finite range | −970.459 | −989.263 | | −831.418 | −844.522 | | −522.013 | |
| Coulomb energy (MeV) | 38.487 | 38.306 | | 33.517 | 33.216 | | 16.746 | |
| rms radius (fm) | 3.034 | 3.043 | 3.360 | 2.958 | 2.988 | 3.231 | 2.629 | 2.822 |

deformations has only been studied in full three-dimensional TDHF calculations[9] for the $^{12}C+^{12}C$ reaction for different relative orientations of the deformed ground state solutions of $^{12}$C and leads to substantial differences in the fusion cross sections.

The initial harmonic oscillator configurations for $^{16}$O, $^{24}$Mg, and $^{27}$Al are listed in Table I. The resulting bulk properties of these nuclei are summarized in Table II, where, for comparison, we have also listed the results for deformed HF solutions of $^{27}$Al and $^{24}$Mg. The oscillator length parameter *b* used is 1.79 fm (corresponding to $\hbar\omega = 13$ MeV). This choice of *b* gives optimum agreement between the calculated and the experimental binding energies for $^{16}$O, $^{27}$Al, and $^{24}$Mg nuclei.

## IV. FUSION RESULTS

We have performed TDHF calculations for the study of fusion cross sections in the $^{16}O+^{27}Al$ reaction at laboratory bombarding energies rang-

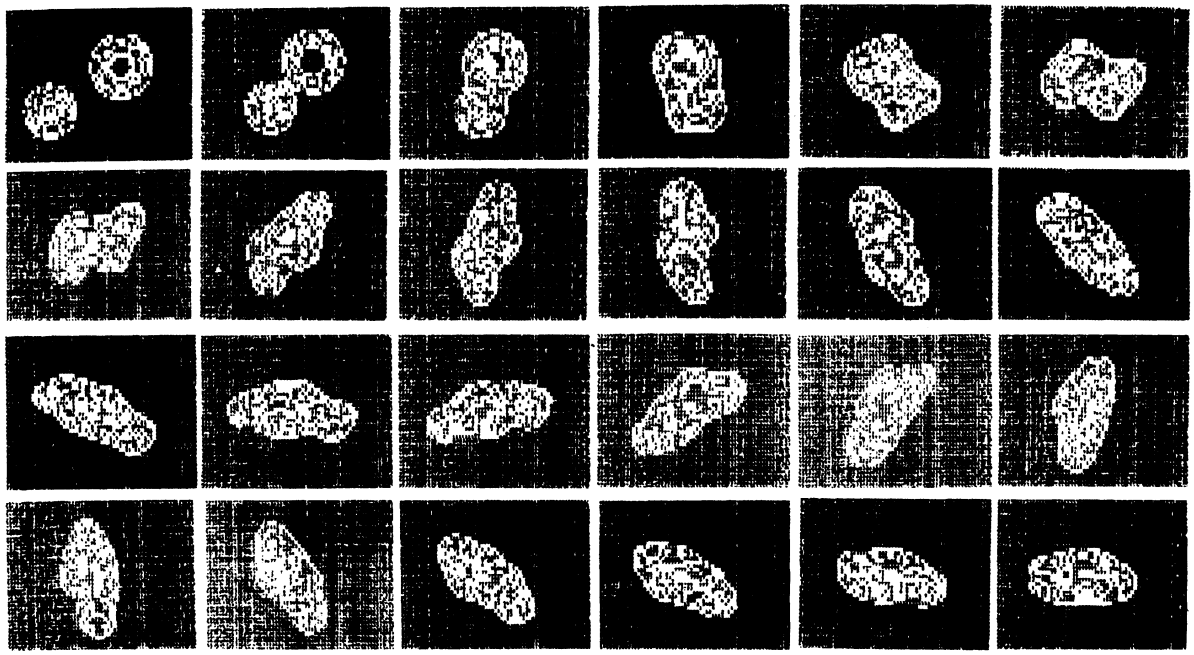

FIG. 1. A typical fusion event. Plotted are the contour plots of the time-dependent density in the reaction plane, for the $^{16}O+^{27}Al$ reaction at $E_{lab}=170$ MeV and for $l=42$. The first and second frames correspond to times $t=0$ and $2\times10^{-22}$ sec, respectively, while the subsequent pictures are in time steps of $10^{-22}$ sec.

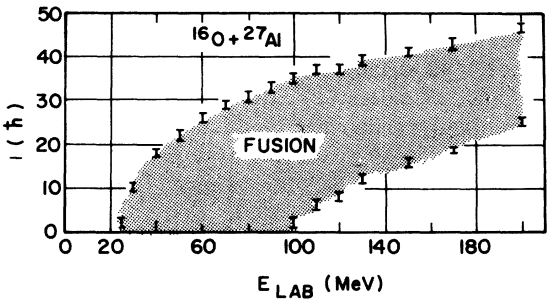


FIG. 2. Lower and upper angular momentum limits to fusion in the $^{16}O+^{27}Al$ reaction. The error bars indicate the uncertainty of 2 in angular momentum.

ing from 25 to 200 MeV and for the $^{16}O+^{24}Mg$ reaction in the range 25 to 100 MeV and also at $E_{lab}$ = 200 MeV. The calculations have been made at various impact parameters or entrance channel angular momentum $l\hbar$ for a specified bombarding energy and the corresponding fusion or nonfusion events identified. Our operational definition of fusion is an event in which the compound system undergoes at least one rotation. In a few cases, we have followed the system up to two or three rotations.

Figure 1 shows a typical TDHF fusion event. Here we display contour plots of the time dependent densities in the reaction plane for the $^{16}O+^{27}Al$ reaction at $E_{lab}$ = 170 MeV and for $l$ = 42. At time $t$ = 0, the separation distance between the ions is 12 fm. As the ions approach each other, a neck is formed and eventually the compound system undergoes damped oscillations and rotations which persist for a long time and suggest fusion behavior. For bombarding energies in the range 25 MeV $\leq E_{lab} \leq$ 200 MeV for the $^{16}O+^{27}Al$ collision we have determined the maximum fusion angular momenta $l_>$ with a precision of 2. However, above $E_{lab}$ = 100 MeV, low impact parameter trajectories do not fuse but lead to highly inelastic events. The values of the upper $l_>$ and the lower $l_>$ angular momentum limits to fusion in the $^{16}O+^{27}Al$ reaction are given in Fig. 2. For this reaction, we notice fusion for all $l$ = 0 paths until an energy $E_{lab}$ = 100 MeV and a rapid increase in $l_>$ up to $E_{lab}$ = 80 MeV beyond which $l_>$ and $l_<$ increase rather slowly. At $E_{lab}$ = 200 MeV, $l_>$ = 46 is 20% larger than the liquid drop limit of 39 for this system.[31] In case of the $^{16}O+^{24}Mg$ reaction the fusion trajectories are identified with a precision of one for an energy range of 25 MeV $\leq E_{lab} \leq$ 100 MeV. At $E_{lab}$ = 100 MeV, all impact parameters with $l \leq 2$ correspond to nonfusion events.

The fusion cross section is then computed using the sharp cutoff formula

$$\sigma_f = \frac{\pi\hbar^2}{2\mu E_{lab}} \frac{m_t + m_p}{m_t}[(l_> + 1)^2 - (l_< + 1)^2],$$

where $\mu$ is the reduced mass of the system, and $m_p$ and $m_t$ are the projectile and target masses, respectively. The TDHF fusion excitation functions for the $^{16}O+^{27}Al$ and $^{16}O+^{24}Mg$ reactions are compared with the experimental data[26-29] in Figs. 3 and 4, respectively. The calculations reproduce the magnitude and gross shape of the experimental curve. At intermediate energies the TDHF points lie above the experimental points as previously observed in other TDHF calculations.[6,10] Note, however, that in the $^{16}O+^{27}Al$ reaction at higher bombarding energies, although the experimental data have large errors, the calculations do reproduce the observed decreasing trend in $\sigma_f$ with increasing bombarding energy. In TDHF calculations this decrease in $\sigma_f$ occurs due to lack of fusion in the lower partial waves. It is interesting to notice that at $E_{lab}$ = 170 MeV,

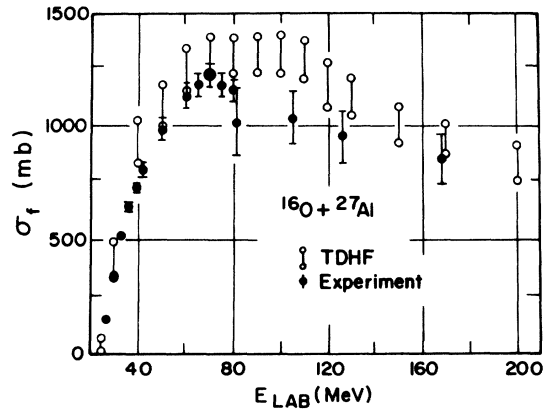


FIG. 3. Calculated and experimental fusion excitation functions for the $^{16}O+^{27}Al$ reaction (experimental data are from Refs. 26–28). The lower and upper calculated fusion limits are obtained from Fig. 2.

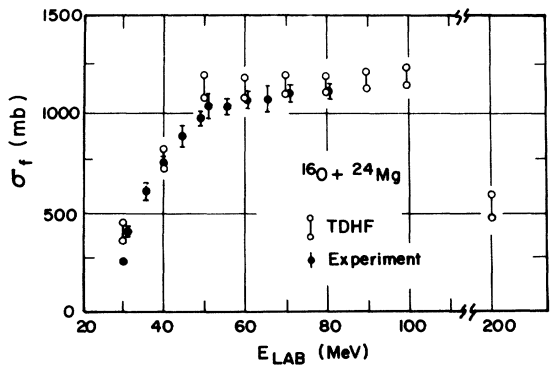


FIG. 4. Fusion excitation function for the $^{16}O+^{24}Mg$ reactions as in Fig. 3. Experimental data are from Ref. 29.

nearly 40% of the reaction cross section corresponds to nonfusion events. In the case of the $^{16}O+^{24}Mg$ reaction at $E_{lab}=200$ MeV all partial waves up to $l=26$ and those above $l=42$ lead to nonfusion events yielding $\sigma_f=633$ mb.

The validity of the two dimensional frozen approximation has recently been questioned for high energy collisions.[10] In $^{28}Si+^{28}Si$ collisions at c.m. energies of 1.1–1.3 MeV per particle above the Coulomb barrier spurious islands of nonfusion events were found in the fusion region. Accordingly we have also investigated the inelastic regions of entrance channel angular momentum in $^{16}O+^{27}Al$ at $E_{lab}=175$ MeV and in $^{16}O+^{24}Mg$ and $E_{lab}=200$ MeV. These reactions are, respectively, 2.0 and 2.5 MeV per particle above the Coulomb barrier in the center of mass, which are considerably higher than those studied in Ref. 10. In Fig. 5 the $^{16}O+^{27}Al$ c.m. scattering angle is shown as a function of entrance channel angular momentum $l$. The fusion region in our calculations appears as a continuous function of $l$ between the upper and lower limits of 42 and 19, respectively, with grazing occurring slightly above $l=54$. We have evaluated the deflection function at angular momentum intervals $\Delta l=4$ or less and find no evidence for the "fractioning" of the fusion cross section in this case. We have also studied the scattering of $^{16}O+^{24}Mg$ for angular momentum below $l_>=42$ at intervals of $\Delta l=5$. Again we find no islands of inelastic scattering in the fusion region. Our results are consistent with those of Ref. 16 for $^{16}O+^{93}Nb$ at 1.08 MeV per particle above the Coulomb barrier, where a continuous region of fusion is also found.

One of the characteristic features that has emerged from the TDHF studies is the transparency behavior of the system for small impact parameters and at relatively high bombarding energies. Such a behavior is seen not only in the studies of lighter heavy ion collisions but also in the heavier systems.[30] This is a feature of the long mean free path implicit in the TDHF approximation. This transparency is dramatically seen in the head-on collisions between mass asymmetric ions at energies where the lower partial waves do not fuse. Figure 6 illustrates this behavior in the case of the $^{16}O+^{24}Mg$ reaction at $E_{lab}=200$ MeV and $l=0$ where the projectile-like fragment is seen to pass through the target-like fragment.

In summary, we have shown that the TDHF calculations with the two-dimensional frozen approximation provide good agreement between the calculated and observed magnitude and shape of the fusion excitation function in the $^{16}O+^{27}Al$ and

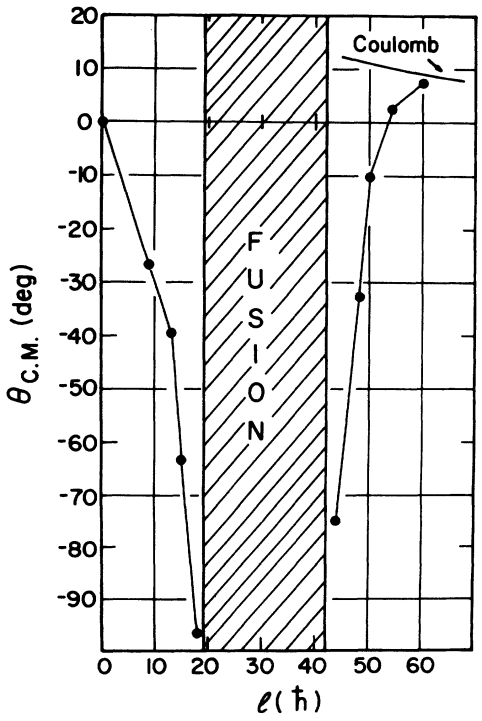


FIG. 5. Center of mass scattering angle $\theta_{c.m.}$ as a function of entrance channel angular momentum $l$ for $^{16}O+^{27}Al$ at $E_{lab}=175$ MeV. The upper and lower limits for fusion are 42 and 19, respectively.

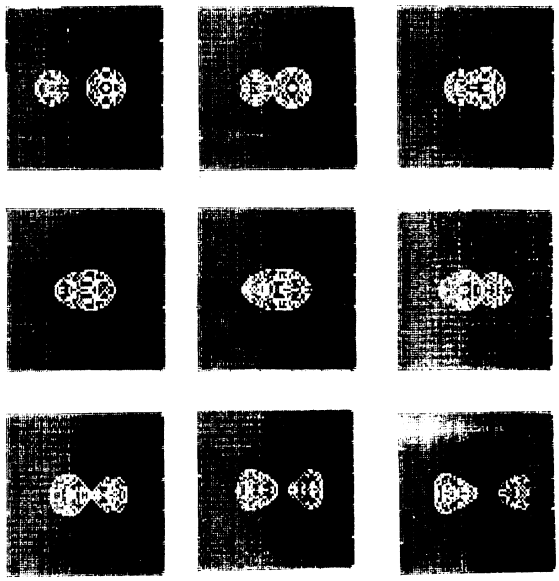

FIG. 6. Contour plots of the time-dependent density in the $^{16}O+^{24}Mg$ reaction at $E_{lab}=200$ MeV for $l=0$. The densities are plotted at times of 0, 0.08, 0.16, 0.20, 0.26, 0.32, 0.38, 0.44, and 0.50, in units of $10^{-21}$ sec, reading from upper right to left, respectively. Note at the end of the reaction that the projectile-like fragment passes through the target-like fragment.

$^{16}O+^{24}Mg$ reactions. Our results, obtained using the finite-range Skyrme II force, contain no new features not found in earlier work using simpler forces:

(1) Upper angular momentum limits $l_>$, which agree with the liquid drop fusion limits to within 20%.

(2) A rapid decrease in the fusion cross sections at high energy due to the absence of fusion events in low partial waves. This decrease is much faster than $1/E_{c.m.}$.

In our use of the frozen approximation and the static filling approximation we find no evidence for the existence of islands of spurious nonfusion.

ACKNOWLEDGMENTS

We would like to thank J. W. Owen for his initial collaboration and M. A. Nagarajan and J. M. Irvine for useful discussions. The calculations reported here have been performed on the Cray-1 computer at the SRC Daresbury Laboratory and we would like to thank the computer staff for their help and cooperation. Typical times for these systems on the Cray are 4 and 10 min, respectively, for inelastic and fusion trajectories. This research was sponsored in part by the division of Physical Research, U.S. Department of Energy under Contract No. DE-AC02-76ER3074, by the U. S. National Science Foundation under Grant No. PHYS 77-21602, and by the U. K. Science Research Council.

[1]P. Bonche, S. E. Koonin, and J. W. Negele, Phys. Rev. C 13, 1226 (1976).
[2]R. Y. Cusson, R. K. Smith, and J. Maruhn, Phys. Rev. Lett. 36, 1166 (1976).
[3]H. Flocard, S. E. Koonin, and M. S. Weiss, Phys. Rev. C 17, 1682 (1978).
[4]P. Bonche, B. Grammaticos, and S. E. Koonin, Phys. Rev. C 17, 1700 (1978).
[5]K. T. R. Davies, H. T. Feldmier, H. Flocard, and M. S. Weiss, Phys. Rev. C 18, 2631 (1978).
[6]S. J. Krieger and K. T. R. Davies, Phys. Rev. C 18, 2567 (1978); 20, 167 (1979).
[7]A. K. Dhar and B. S. Nilsson, Nucl. Phys. A315, 445 (1979).
[8]A. K. Dhar, B. S. Nilsson, and H. Jagman, Niels Bohr Institute Report No. NBI-78-31.
[9]B. S. Nilsson, A. K. Dhar, and S. E. Koonin (unpublished).
[10]P. Bonche, K. T. R. Davies, B. Flanders, H. Flocard, B. Grammaticos, S. E. Koonin, S. J. Krieger, and M. S. Weiss, Phys. Rev. C 20, 641 (1979).
[11]K. T. R. Davies, V. Maruhn-Rezwani, S. E. Koonin, and J. W. Negele, Phys. Rev. Lett. 41, 632 (1978).
[12]A. K. Dhar and B. S. Nilsson, Phys. Lett. 77B, 50 (1978); A. K. Dhar, Phys. Rev. Lett. 42, 1124 (1979).
[13]K. T. R. Davies, K. R. Sandhya Devi, and M. R. Strayer, Phys. Rev. C 20, 1372 (1979).
[14]A. K. Dhar, B. S. Nilsson, K. T. R. Davies, and S. E. Koonin (unpublished).
[15]R. Y. Cusson and H. W. Meldner, Phys. Rev. Lett. 42B, 694 (1978); R. Y. Cusson, H. W. Meldner, and H. Stöcker (unpublished).
[16]K. R. Sandhya Devi, M. R. Strayer, J. M. Irvine, and K. T. R. Davies (unpublished).
[17]K. T. R. Davies, H. Flocard, S. J. Krieger, and M. S. Weiss, Nucl. Phys. A342, 111 (1980).
[18]K. R. S. Devi, A. K. Dhar, and M. R. Strayer (unpublished).
[19]P. Hoodbhoy and J. W. Negele, Nucl. Phys. A288, 23 (1977).
[20]V. Maruhn-Rezwani, K. T. R. Davies, and S. E. Koonin, Phys. Lett. 67B, 134 (1977); S. E. Koonin, K. T. R. Davies, V. Maruhn-Rezwani, H. Feldmeier, S. J. Krieger, and J. W. Negele, Phys. Rev. C 15, 1359 (1977).
[21]S. E. Koonin and K. T. R. Davies (unpublished).
[22]K. R. Sandhya Devi and M. R. Strayer, Phys. Lett. 77B, 135 (1978); J. Phys. G 4, L97 (1978); K. R. Sandhya Devi, M. R. Strayer, and J. M. Irvine, *ibid.* 5, 281 (1979).
[23]S. E. Koonin, B. Flanders, H. Flocard, and M. S. Weiss, Phys. Lett. 77B, 13 (1978).
[24]B. Flanders, P. Bonche, S. E. Koonin, and M. S. Weiss (unpublished).
[25]K. R. Sandhya Devi and M. R. Strayer (unpublished).
[26]J. Dauk, K. Lieb, and A. Kleinfeld, Nucl. Phys. A241, 170 (1975).
[27]R. Kozub, N. Lu, J. Miller, D. Logan, T. Debiak, and L. Kowalski, Phys. Rev. C 11, 1497 (1975).
[28]B. Back, R. Betts, C. Gaarde, J. Larsen, E. Michelsen, and Tai Kuang-Hoi, Nucl. Phys. A285, 317 (1977).
[29]S. Tabor, D. Geesaman, W. Henning, D. K ır, K. Rehn, and F. Prosser, Phys. Rev. C 17, 2136 (1978).
[30]K. T. R. Davies, K. R. Sandhya Devi, and M. R. Strayer, Phys. Rev. Lett. 44, 23 (1980).
[31]S. Cohen, F. Plasil, and W. J. Swiatecki, Ann. Phys. (N.Y.) 82, 557 (1974).

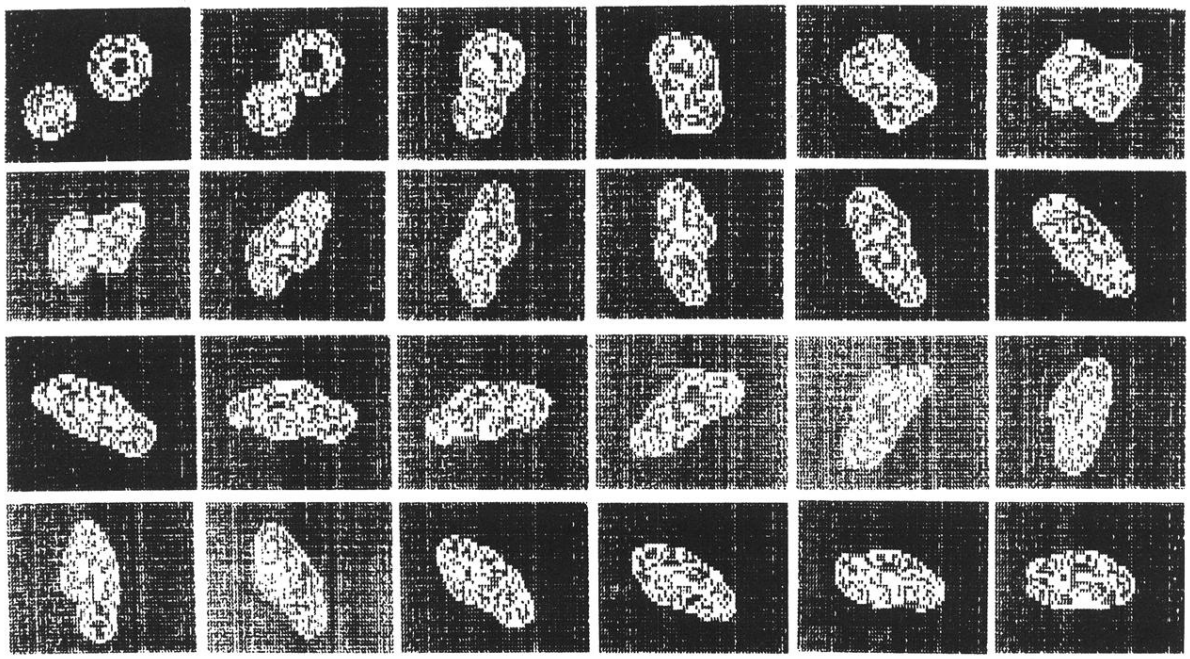

FIG. 1. A typical fusion event. Plotted are the contour plots of the time-dependent density in the reaction plane, for the $^{16}O + {}^{27}Al$ reaction at $E_{lab} = 170$ MeV and for $l = 42$. The first and second frames correspond to times $t = 0$ and $2 \times 10^{-22}$ sec, respectively, while the subsequent pictures are in time steps of $10^{-22}$ sec.

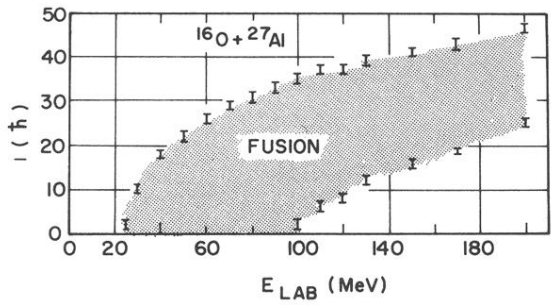


FIG. 2. Lower and upper angular momentum limits to fusion in the $^{16}O + ^{27}Al$ reaction. The error bars indicate the uncertainty of 2 in angular momentum.

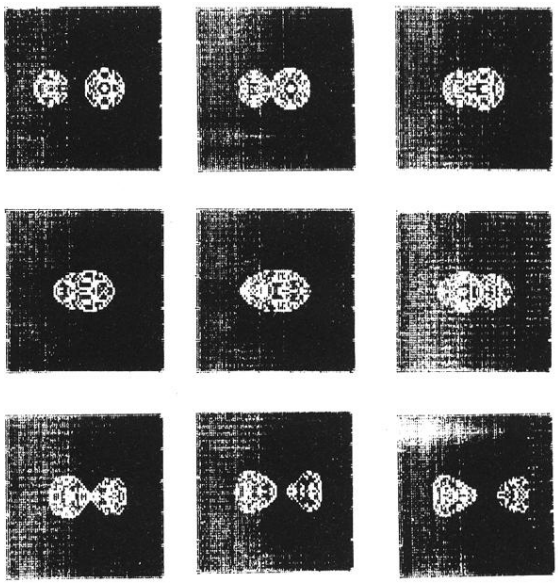

FIG. 6. Contour plots of the time-dependent density in the $^{16}O + ^{24}Mg$ reaction at $E_{lab} = 200$ MeV for $l = 0$. The densities are plotted at times of 0, 0.08, 0.16, 0.20, 0.26, 0.32, 0.38, 0.44, and 0.50, in units of $10^{-21}$ sec, reading from upper right to left, respectively. Note at the end of the reaction that the projectile-like fragment passes through the target-like fragment.